scientific reports

Check for updates

OPEN

Native CFTR codon bias controls translation rate to balance off-pathway aggregation and channel function by conformational imprinting

Jae Seok Yoon[1]✉, Hongyu Li[2], Yonjung Kim[3], Hideki Shishido[1], David N. Sheppard[2]✉, Min Goo Lee[3] & William R. Skach[4,5]✉

Protein folding in vivo is biologically tuned to minimize off-pathway events and optimize native folding outcomes. A key factor in this process is biased synonymous codon usage, in which synonymous codons modulate local translation rate while maintaining the native amino acid sequence. Here, we demonstrate that native codon usage within the first nucleotide-binding domain (NBD1) of the cystic fibrosis transmembrane conductance regulator (CFTR) induces a translational pause during a critical window of synthesis that affects CFTR folding, processing, and function. Eliminating this pause by substituting synonymous codons increased the aggregation propensity of immature CFTR and induced conformational and functional changes that persisted during CFTR processing and plasma membrane expression. Interestingly, the resulting mature CFTR protein at the plasma membrane exhibited enhanced ATP-dependent chloride channel gating. Thus, during protein synthesis, cotranslational events dictated by codon usage can imprint persistent conformational and functional properties upon CFTR. Our findings suggest that CFTR codon usage has evolved and adapted to balance a compromise between protein aggregation and a modest loss of channel function.

The primary sequence of amino acids in a polypeptide is a key determinant of protein folding that gives rise to native three-dimensional structure and ultimately protein function[1]. In cells, however, protein folding begins cotranslationally from N- to C-terminus as the nascent polypeptide emerges from the ribosome during the process of translation[2,3]. Vectorial and length-dependent protein folding is therefore influenced not only by the sequence of amino acids but also by cotranslational constraints such as ribosome effects, molecular crowding, cellular chaperone binding, and translation rate[4–6]. Cotranslational folding is increasingly recognized as beneficial for complex proteins by reducing misfolding and promoting native folding pathways[7,8].

For certain complex proteins, such as the Cystic Fibrosis Transmembrane conductance Regulator (CFTR), folding and maturation involve multiple processes. Full-length CFTR, a 1,480-amino acid membrane protein, requires correct folding of each of its peptide domains: two transmembrane domains (TMD1 and 2), two nucleotide-binding domains (NBD1 and 2), and a partially disordered regulatory (R) region, followed by cooperative assembly of these domains into the final folded structure (Fig. 1A)[9–11]. Upon maturation, CFTR undergoes complex glycosylation and is trafficked to the apical membrane of epithelial cells, where it functions as a chloride channel regulated by cAMP-dependent phosphorylation[12–14]. Among its domains, NBD1 folding is particularly critical to achieve the native conformation. Misfolding of F508del CFTR, the most prevalent cystic fibrosis (CF)-causing *CFTR* variant (c.1521-1523delCTT), for instance, originates in NBD1, causing defects in both local folding and allosteric domain assembly[13,15,16].

We previously showed that native folding of NBD1 involves sequential and coordinated compaction of three canonical subdomains: the N-terminal, α-helical, and β-sheet core subdomains (Fig. 1A)[17–19]. During de novo folding, the N-terminal subdomain folds rapidly and serves as a metastable scaffold for subsequent folding

[1]CFFT Lab, Cystic Fibrosis Foundation, 44 Hartwell Ave., Lexington, MA 02421, USA. [2]School of Physiology, Pharmacology and Neuroscience, University of Bristol, Bristol, UK. [3]Department of Pharmacology, Brain Korea 21 PLUS Project for Medical Sciences, Yonsei University College of Medicine, Seoul, Korea. [4]Cystic Fibrosis Foundation, Bethesda, MD, USA. [5]Salem, OR, USA. ✉email: jyoon@cff.org; D.N.Sheppard@bristol.ac.uk; wskach@gmail.com

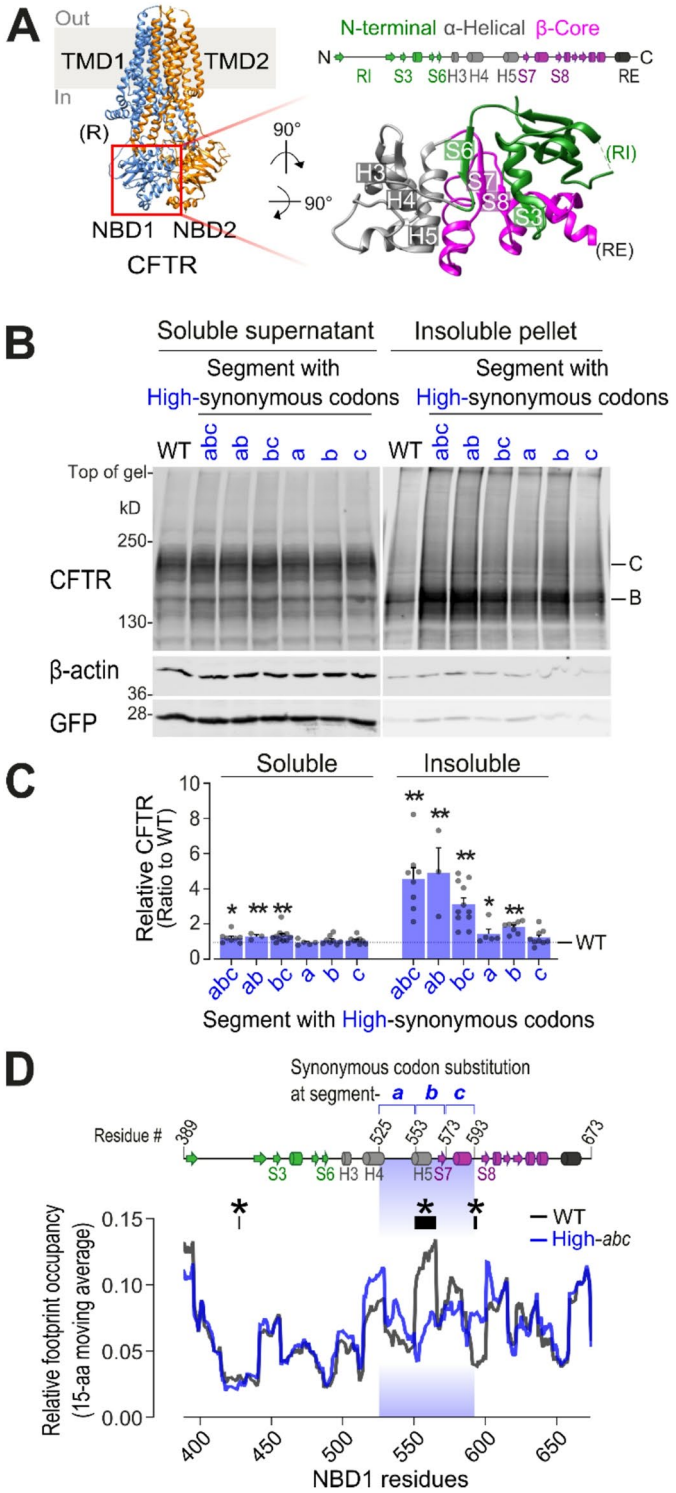

events. By contrast, the ribosome-induced delay in α-helical subdomain folding facilitates proper formation of the buried β-sheet core[19]. Two CF-causing *CFTR* variants, A455E (c.1364C > A) and L558S (c.1673T > C), transiently disrupt the closely coupled decoding kinetics between the α-helical and β-sheet core subdomains, leading to misfolding of NBD1 and, consequently, full-length CFTR[20]. During this critical window of α-helical and β-sheet core subdomain synthesis, codon usage is predicted to slow ribosome decoding kinetics (translation rate)[19,21]. Introducing synonymous codon substitutions, which presumably increase the translation rate in this region without altering the amino acid sequence, leads to enhanced aggregation propensity of the newly synthesized CFTR, despite no significant change in overall protein processing[19]. Collectively, these findings suggest that cotranslational events occurring during NBD1 synthesis play a critical role in CFTR biogenesis.

During de novo protein synthesis in cells, the speed of ribosome translation along the mRNA is not uniform, and local variations can influence cotranslational folding and functional expression[22–24]. Translational slowdown or pausing is generally thought to allow nascent polypeptides more time to fold correctly, engage with ribosome-

◀**Fig. 1**. Codon usage in NBD1 affects CFTR aggregation propensity. (**A**) Left, Orthogonal stereo ribbon representation of phosphorylated, ATP-bound human CFTR with the E1371Q mutation [Protein Data Bank (PDB) ID: 6MSM][10], generated using UCSF Chimera[65]. The unstructured R region is denoted in parentheses. The position of the plasma membrane is shown with the intracellular (In) and extracellular (Out) sides identified. Right, Magnified view of NBD1 (domain enclosed by a red box in the CFTR structure), rotated 90° about both the x- and y-axes relative to the CFTR structure. Secondary structural elements of NBD1 are indicated above the magnified view, with α-helices shown as cylinders and β-strands as filled arrows. Subdomains of NBD1 are color-coded: N-terminal (green), α-helical (gray), and β-sheet core (magenta). Helices H3-H5 in the α-helical subdomain and β-strands S3 and S6-S8 in the β-sheet core subdomain are labeled. The locations of the regulatory insertion (RI) and regulatory extension (RE) are also denoted by labels in parentheses. (**B**) Representative immunoblot of WT CFTR and variants bearing High-efficiency synonymous codon substitutions showing immature (band B) and mature (band C) CFTR protein in radioimmunoprecipitation assay (RIPA)-soluble and insoluble fractions. β-actin and co-expressed GFP serve as loading and transfection controls, respectively. Original uncropped blots are presented in Fig. S1. (**C**) Summary data show fold changes in total (band B + band C) relative to WT (indicated by dotted line) for CFTR variants bearing High-efficiency synonymous codon substitutions. Symbols show individual values and columns are means ± SEM ($n = 3$–11 independent experiments per variant); * $P < 0.05$ and ** $P < 0.01$ vs. WT CFTR by two-tailed Student's t-test. (**D**) Relative ribosome occupancy across NBD1 (residues 389–673), calculated with a 15-amino acid moving window average, for WT CFTR (black) and the CFTR construct with High-codons in segment-*abc* (blue). Secondary conformations of NBD1 are indicated above the graph, with α-helices shown as cylinders and β-strands as filled arrows. The light blue shaded region (residues 525–593) marks the segment changed in the CFTR construct with High-codons in segment-*abc*. Data are the means of five independent experiments per construct. Asterisks denote residues with statistically significant differences in ribosome occupancy between WT and the CFTR construct with High-codons in segment-*abc* (*$P < 0.05$; two-tailed Student's t-test). Ribosome profiling data shown in (**D**) are also represented in Figs. 2, 3A, S2, and S3A,B.

associated chaperones, and undergo co- or post-translational modifications, thereby promoting on-pathway folding, maturation, and intracellular processing[22,25]. Conversely, a prolonged pause may reduce translational fidelity through frameshifting or amino acid misincorporation and increase exposure to mRNA surveillance and premature degradation[26–29]. Thus, factors such as codon usage, tRNA availability, mRNA structure, post-transcriptional and translational modifications, and protein sequence must be coordinated to maintain the optimal speed of ribosomal decoding[30–34].

Here, we employed ribosome profiling to examine translation dynamics across the CFTR transcript and identified several instances of translational pausing, including one during the critical period of NBD1 cotranslational folding. To investigate the influence of translation rate on early off-pathway CFTR aggregation and its impacts on the conformational properties of NBD1 and CFTR, we manipulated codon usage in this specific region. Furthermore, we conducted studies using the patch-clamp technique to evaluate the consequences of non-native synonymous codon usage for CFTR channel function. Our results indicate that while modulating codon usage in this region can enhance CFTR function, it also increases the risk of propensity for early aggregation.

Results

Codon usage in the NBD1 α-helical subdomain affects CFTR aggregation propensity

The NBD1 β-sheet core subdomain contains four parallel β-strands (S3, S6, S7, and S8: residues 453–458, 488–491, 568–572, and 599–603, respectively) buried within the hydrophobic interior of the domain (Fig. 1A)[10,17]. During NBD1 synthesis, these four β-strands are translated non-contiguously: S3 and S6 are synthesized first, then, after the α-helical subdomain, S7 and S8. Thus, correct β-sheet folding requires insertion of S7 and S8 between the preexisting S3 and S6 following synthesis of the α-helical subdomain. Our previous studies using fluorescence resonance energy transfer (FRET)[18–20] showed that these cotranslational folding events are temporally coupled with translation, facilitating efficient β-sheet formation. Codon usage within residues 525–593, which span the α-helical and β-sheet core subdomains, is enriched in codons predicted to have low translation efficiency (Table S1), designated here as 'Low-efficiency' or "Low" codons, due to limited isoacceptor tRNA availability and wobble base-pairing[19,21]. Synonymous substitutions with 'High-efficiency' (or "High") codons, defined as those predicted to have high translation efficiency, resulted in increased aggregation propensity of newly synthesized CFTR protein[19]. Metabolic pulse-chase labeling experiments revealed that the increased aggregation observed in CFTR with High-efficiency codons, although overall protein processing efficiency remained unchanged, is likely due to misfolded intermediates being more prone to aggregation or to delayed clearance of aggregates, rather than an increase in misfolding during synthesis[19].

To better understand how codon usage influences this critical window of NBD1 cotranslational folding, we divided the 525–593 region into three subregions: segment-*a* (525–552), segment-*b* (553–572), and segment-*c* (573–593) (Fig. 1B–D). We introduced High-codons into each segment, ensuring that the number of synonymous codon substitutions per construct was comparable (18–20 codons) (Table S1). WT and High-codon constructs were exogenously expressed in HEK293 cells, lysed in radioimmunoprecipitation assay (RIPA) buffer, and separated into soluble supernatant and insoluble pellet by centrifugation. Insoluble pellets containing aggregated CFTR were solubilized in 1% (w/v) sodium dodecyl sulfate (SDS) for subsequent analysis as previously described[19]. β-actin and co-expressed GFP were used as loading and transfection controls,

respectively. Consistent with our previous findings[19], all High-codon constructs showed similar levels of soluble, mature CFTR protein (band C) (Figs. 1B,C and S1), indicating that global processing efficiency was not impaired. By contrast, the amount of insoluble, immature CFTR protein (band B) varied depending on the segment (Figs. 1B,C and S1). Notably, constructs bearing High-codons within segment-*b* (*abc*, *ab*, *bc,* and *b*-alone) consistently showed increased aggregation of immature CFTR relative to WT. These findings suggest that codon usage within segment-*b* includes an important determinant of the aggregation of immature CFTR protein.

To assess the relationship between CFTR codon usage and translation rate, we performed ribosome profiling of WT and High-codons in segment-*abc* constructs (GEO: GSE305005). Ribosome footprint libraries from mRNA fragments protected by actively translating ribosomes (Fig. S2)[35,36] were prepared without translation inhibitors to avoid any potential bias in ribosome occupancy[37]. Footprints were mapped onto the CFTR coding sequence (CDS) based on A-site codon identity (see "Methods") to generate the 15-amino acid moving average of ribosome footprint occupancy across NBD1 (Fig. 1D). When compared to WT, the CFTR construct with High-codons in segment-*abc* showed a substantial reduction in footprint density within segment-*b*. As ribosome footprint occupancy is inversely correlated with the relative translation rate (i.e. a slower rate results from increased ribosome dwell time at specific codons), this reduction suggests that High-efficiency codon substitutions elicit a transient increase in translation rate in segment-*b*. These results support the idea that native codon usage within this region slows translation and that disruption of these decoding kinetics may contribute to the observed increase in immature CFTR aggregation.

Translational pauses occur at specific codons during CFTR synthesis

To examine how individual codons affect translation rate across the CFTR CDS, we assessed codon-level ribosome footprint occupancy through ribosome profiling. We exogenously overexpressed the WT CFTR construct in HEK293 cells to obtain sufficient ribosome footprints for this single-transcript analysis. This approach yielded an average of ~ 10,500 footprints per sample preparation across five independent replicates (range: about 2600–33,000). Mapping of ribosome footprints displayed a characteristic triplet periodicity along the CFTR CDS (Fig. 2A), consistent with transcriptome-wide patterns (Fig. S2), confirming that the data reflect actively translating ribosomes[38].

Ribosome occupancy was highly non-uniform across the CFTR CDS, with certain codons exhibiting substantially higher occupancies than others, characteristic of transient translational pauses (Fig. 2B). For this analysis, we arbitrarily defined a translational pause as codons with footprint occupancy greater than tenfold above the transcript-wide average. This criterion identified eleven discrete pause sites within the 1,480-amino acid residue CFTR CDS, nine of which occurred at either Leu(UUA) or Glu(GAA) codons. To further explore codon-specific translational pauses across the CFTR CDS, we visualized ribosome occupancy across all 61 sense codons (Fig. 2C). While UUA and GAA were overrepresented among pause sites, most instances of these codons, 31 out of 37 for UUA and 60 out of 63 for GAA, were not identified as pauses. These findings suggest that while certain codons might preferentially induce a translational pause, sojourns at a given codon are not absolute and are likely influenced by additional factors beyond codon identity[25,32,39].

Transcript-encoded pauses at Leu558 reduce CFTR aggregation

One of the prominent translational pauses across the CFTR CDS occurred at Leu558(UUA), located within segment-*abc* of NBD1 (Fig. 2B) and the site of a CF-causing *CFTR* variant (L558S), which transiently disrupts NBD1 decoding kinetics[20]. To investigate the effect of synonymous codon substitutions on ribosome occupancy within this region, we analyzed the CFTR construct with High-codons in segment-*abc*, in which 57 out of 69 codons (~ 83%) were substituted with High-efficiency codons (Fig. 3A and Table S1). While most substitutions had minimal impact on occupancy relative to their WT counterparts (Figs. 3A and S3A,B), six residues (Asp537, Leu558, Ala559, Ala561, Lys564, and Thr582) showed statistically significant changes. Among these six residues, Ala561 exhibited increased occupancy, whereas the others showed decreased occupancy, consistent with augmented ribosome decoding at those codons. Notably, the most dramatic change occurred at Leu558, where the UUA(native)-to-CUC(High) codon substitution eliminated the translational pause (Figs. 3A and S3A,B).

To assess the role of this pause, we first introduced a single synonymous UUA-to-CUC codon substitution at Leu558 in the WT construct. Consistent with prior observations (Figs. 1B,C, 2B, and 3A), this substitution eliminated the native pause (Fig. S3C) without affecting CFTR band C processing (Figs. 3B, lanes 1–2; 3C and S4). Although Leu558(CUC) alone caused a modest increase in aggregation of immature CFTR (Figs. 3B, lanes 5–6; 3C and S4), reintroduction of the native UUA codon at Leu558 into the CFTR construct with High-codons in segment-*abc* partially restored the pause (Fig. S3D) and markedly reduced the aggregation of immature CFTR by this construct (Figs. 3B, lanes 7–8; C and S4). These findings indicate that the native translational pause at Leu558 contributes to preventing aggregation of immature CFTR, but that additional synonymous codons within segment-*abc* also modulate this effect. Together, these results provide further evidence that transcript-encoded codon bias can cooperate to tune NBD1 folding and reduce early off-pathway aggregation during CFTR biogenesis.

Synonymous substitutions affect the conformational properties of newly synthesized NBD1

We asked whether High-codon substitutions might locally alter the conformational properties of NBD1, even though such subtle changes do not significantly impact global CFTR processing efficiency. To test this possibility, we performed immunoprecipitation (IP) assays on newly synthesized NBD1 to assess potential differences in epitope accessibility, using three well-characterized monoclonal CFTR antibodies, 3G11, 7D12, and UNC660. These antibodies recognize defined epitopes in the N-terminal (epitope residues 396–405), α-helical (epitope residues 531–540), and β-sheet core (epitope residues 576–585) subdomains, respectively (Fig. 4A)[40,41].

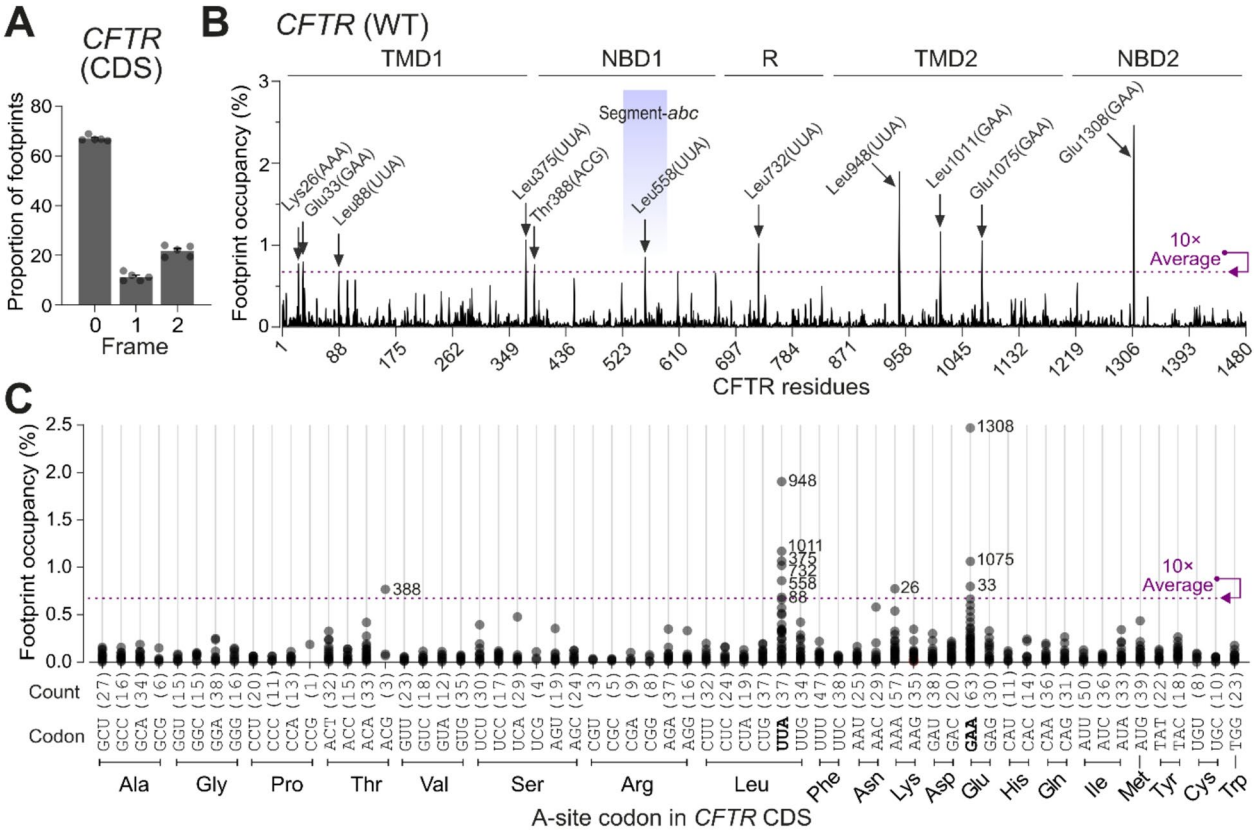

Fig. 2. Ribosome profiling reveals translational pause sites in the CFTR transcript. (**A**) Triplet periodicity of ribosome footprints within the CFTR coding sequence (CDS). The proportion of ribosome footprints (28–30 nt) mapping to each reading frame is shown. Data are means ± SEM (n = 5 independent experiments). (**B**) Ribosome footprint occupancy across the WT CFTR CDS. Ribosome positions were determined based on the codon occupying the A-site (see "Methods"). Arrows indicate eleven amino acid residues with footprint occupancy greater than tenfold the transcript-wide average (dotted line), arbitrarily defined as translational pause sites. Data are the means of five independent experiments. The segment-*abc* region is shaded in light blue. This panel is reproduced in Fig. S3A. (**C**) Footprint occupancy for each of the 61 A-site codons within the WT CFTR CDS. Data are the means of five independent experiments; each filled circle represents footprint occupancy at a single residue. The dotted line indicates the tenfold transcript-wide average with translational pause site residues identified in panel B labeled by their residue number. The occurrence of each codon in the CDS is indicated in parentheses. UUA and GAA codons are highlighted in bold font.

NBD1 constructs containing WT and either High- or Low-codons in segment-*abc* were tested. The construct with Low-codons served as a negative control, as it has negligible effects on protein expression, processing, and aggregation[19]. HEK293 cells heterogeneously expressing NBD1 (residues 389–673, ~30 kDa) were radiolabeled and subsequently lysed, and the RIPA-soluble lysates were equally divided for IP with each antibody. The IP results revealed that WT NBD1 and that with Low-codons in segment-*abc* showed similar levels of protein recovery across all three antibodies (Figs. 4B, lanes 1–2, 4–5, and 7–8; C and S5), indicating no major difference in epitope accessibility. By contrast, NBD1 with High-codons in segment-*abc* exhibited increased recovery with each antibody (Figs. 4B, lanes 3, 6, and 9; C and S5), consistent with elevated expression due to enhanced translation efficiency[19]. Interestingly, when the recovery of NBD1 with High-codons in segment-*abc* was normalized to that of WT NBD1 (3G11: Fig. 4B, lane 3 to 1; 7D12: Fig. 4B, lane 6 to 4; UNC660: Fig. 4B, lane 9 to 7), the recovery with 7D12 was disproportionately higher than with either 3G11 or UNC660 (Fig. 4C), suggesting increased accessibility of the 7D12 epitope in the α-helical subdomain. These results suggest that High-codons in segment-*abc* alter the cotranslational folding pathway of NBD1, resulting in a local conformational change within the α-helical subdomain.

Conformational properties established during cotranslational folding persist throughout CFTR maturation

We next tested whether the increased 7D12 reactivity observed in the isolated NBD1 domain also occurs in full-length CFTR. CFTR constructs with either WT, High-, or Low-codons in segment-*abc* were transiently expressed in HEK293 cells, solubilized in RIPA buffer, and subjected to IP using two monoclonal antibodies: 7D12 (specific to NBD1) and M3A7 (specific to NBD2, epitope residues 1365–1390). As the M3A7 epitope

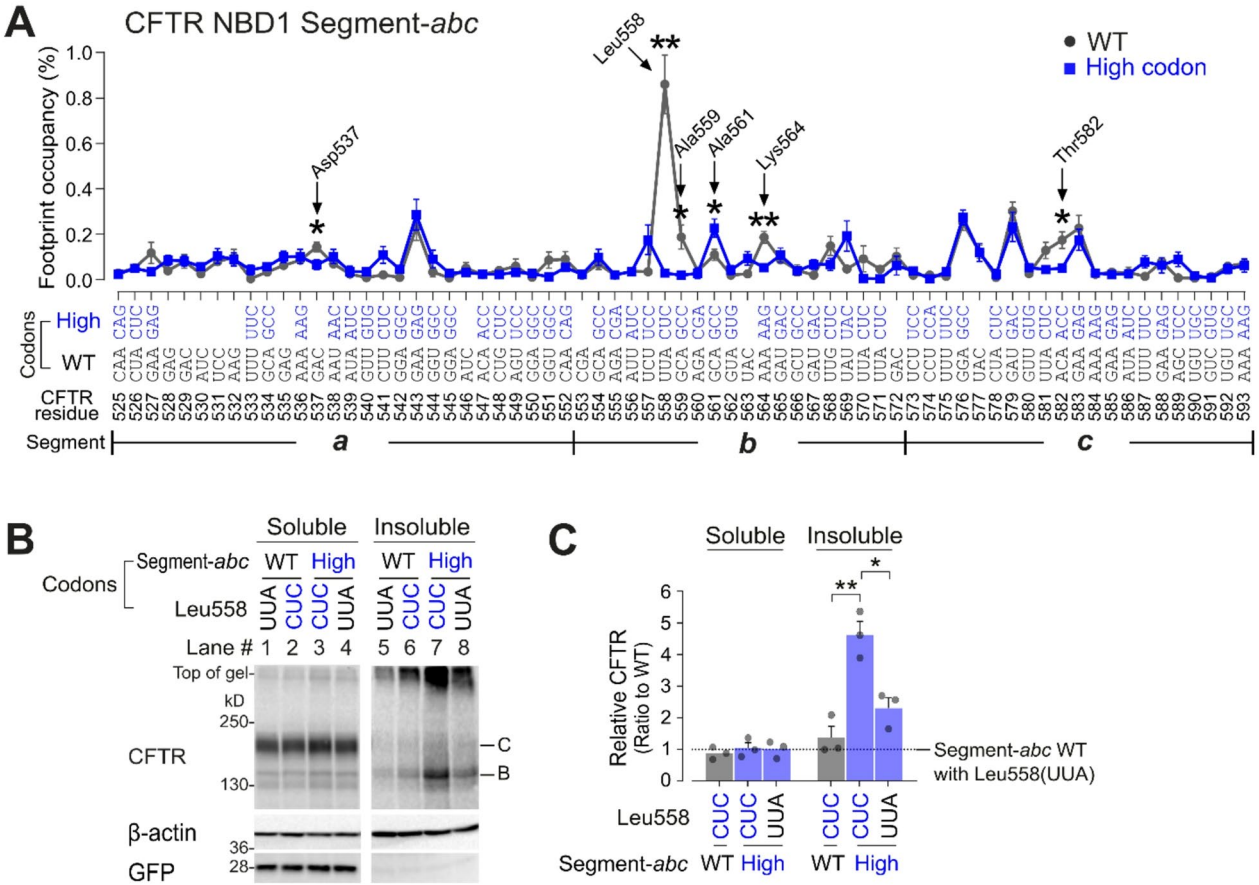

Fig. 3. The translational pause at Leu558 acts cotranslationally to prevent aggregation of CFTR. (**A**) Ribosome footprint occupancy within NBD1 segment-*abc* (residues 525–593) for WT CFTR (black) and the CFTR construct with High-codons in segment-*abc* (blue). Codons substituted in this CFTR construct that differ from WT are indicated by blue letters. Data are means ± SEM ($n = 5$ independent experiments); error bars are smaller than symbol size except where shown. Asterisks indicate residues with a statistically significant difference in footprint occupancy between WT and the CFTR construct with High-codons in segment-*abc* ($^*P < 0.05$ and $^{**}P < 0.01$; two-tailed Student's t-test). (**B**) Representative immunoblots showing expression of WT CFTR and High-efficiency codon variants from RIPA-soluble and -insoluble lysate fractions. Immature (band B) and mature (band C) forms of CFTR protein are indicated. β-actin and GFP serve as loading and transfection controls, respectively. Original uncropped blots are presented in Fig. S4. (**C**) Summary data show fold changes in total (band B + band C) CFTR protein relative to WT CFTR with Leu558(UUA) for High-efficiency codon variants. Symbols show individual values, and columns are means ± SEM ($n = 3$ independent experiments per variant); $^*P < 0.05$ and $^{**}P < 0.01$ vs. CFTR with High-codons in segment-*abc* (two-tailed Student's t-test).

resides in NBD2, it served as a control for overall protein expression. Lysates were equally divided for IP with either 7D12 or M3A7, followed by immunoblotting with 3G11 (Figs. 5A and S6A).

Using both 7D12 (Fig. 5A, lanes 1–2) and M3A7 (Fig. 5A, lanes 4–5), CFTR constructs with either WT or Low-codons in segment-*abc* showed similar recovery of both immature (band B) and mature (band C) CFTR protein (Fig. 5B), consistent with previous results[19]. As expected, recovery of all three constructs was comparable with M3A7 (Fig. 5A, lanes 4–6; B), confirming equivalent expression levels. However, the CFTR construct with High-codons in segment-*abc* showed significantly increased recovery with the 7D12 antibody for both immature (band B) and mature (band C) CFTR protein (Fig. 5A, lane 3; B), indicating that the altered conformation of 7D12 epitope, established during NBD1 synthesis, is preserved throughout CFTR maturation.

To determine whether the codon substitutions directly affect the 7D12 epitope itself (residues 531–540), we examined the CFTR construct with High-codons in segment-*bc*, which contains WT codons for segment-*a* (residues 525–552; where the 7D12 epitope resides) and High-codons for the downstream segment-*bc* (Figs. 1D and 4A). As with the CFTR construct with High-codons in segment-*abc* (Fig. 5A,B), this CFTR construct showed increased 7D12 reactivity (Figs. 5C,D and S6B), suggesting that the change likely occurs in close temporal proximity as segment-*a* emerges from the ribosome during translation of segment-*bc*. These observations imply that synonymous codon changes can affect cotranslational events in a manner that imprints conformational properties retained in the mature CFTR protein.

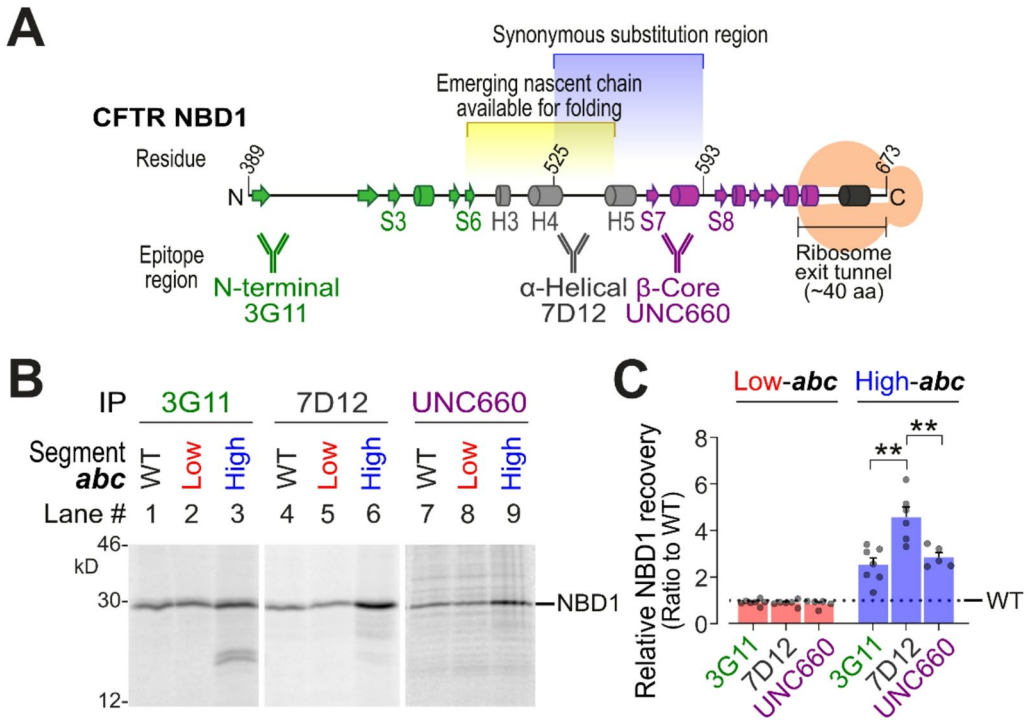

Fig. 4. Alterations in cotranslational events during NBD1 synthesis affect epitope accessibility. (**A**) Schematic overview of immunogenic epitopes recognized by three anti-CFTR NBD1 antibodies (3G11: N-terminal; 7D12: α-helical; UNC660: β-sheet core), mapped onto the NBD1 secondary structure shown in Fig. 1D depicted emerging from the ribosome. The yellow-shaded region represents the nascent polypeptide segment expected to be available for cotranslational folding on emergence from the ribosome as the blue-shaded region (residues 525–593) is being translated. (**B**) Representative immunoprecipitations of metabolically labeled CFTR NBD1 expressed from WT and CFTR NBD1 constructs with Low- and High-codons in segment-*abc* using the three different NBD1-specific antibodies. The position of isolated CFTR NBD1 is indicated. Original uncropped blots are presented in Fig. S5. (**C**) Summary data show the fold changes of the CFTR NBD1 constructs with Low- and High-codons in segment-*abc* relative to WT for each antibody. Symbols show individual values, and columns are means ± SEM ($n = 5–7$ independent experiments per antibody); $^{**}P < 0.01$ vs. 7D12 (two-tailed Student's t-test).

Cotranslational imprinting enhances CFTR channel function

During CFTR channel gating, conformational transitions are regulated by ATP-driven NBD1-NBD2 heterodimerization and ATP hydrolysis-catalyzed dissociation of the NBD dimer, which correspond to channel opening and closing, respectively[42,43]. Because the 7D12 epitope in NBD1 is located near the NBD dimer interface[10,17] (Fig. 6A), we tested whether the altered 7D12 epitope observed in the CFTR construct with High-codons in segment-*abc* might affect channel gating at the single-channel level. Functional analyses comparing WT and the CFTR construct with High-codons in segment-*abc* were independently performed by two research groups with researchers blinded to construct identity. Using different experimental conditions, the two groups studied HEK293 (Fig. 6B–D) and CHO-K1 (Fig. 6E–G) cells heterologously expressing CFTR constructs with the excised inside-out membrane patch configuration of the patch-clamp technique.

Single-channel current amplitudes were indistinguishable between WT and the CFTR construct with High-codons in segment-*abc* using the different cell types and experimental conditions (Fig. 6C and F), indicating comparable ion conductance (Fig. 6C). However, notable differences were observed in channel gating properties despite the different experimental conditions used by the two research groups, which led to different open probability (P_o) values[44–46]. In both HEK293 and CHO-K1 cells, the CFTR construct with High-codons in segment-*abc* had a noticeably higher P_o than WT in the presence of ATP (3 mM) (Fig. 6D and G). Consistent with this finding, analysis of ATP concentration–P_o relationships revealed that the CFTR construct with High-codons in segment-*abc* displayed enhanced ATP sensitivity compared with WT CFTR, as reflected by its increased ATP affinity (lower ATP dissociation constant (K_D)) and efficacy (higher maximal open probability ($P_{o(max)}$)) (WT: $K_D = 281$ μM, $P_{o(max)} = 0.35$, $r^2 = 0.99$; High-*abc*: $K_D = 177$ μM, $P_{o(max)} = 0.46$, $r^2 = 0.94$; determined from Michaelis–Menten fits to mean data). At all ATP concentrations tested, the enhanced ATP sensitivity of the CFTR construct with High-codons in segment-*abc* was manifested by increased frequency and duration of channel openings (Fig. 6E and G). Thus, these results demonstrate that synonymous codon usage in a specific region of NBD1 modulates the conformation of mature CFTR protein to enhance its gating properties.

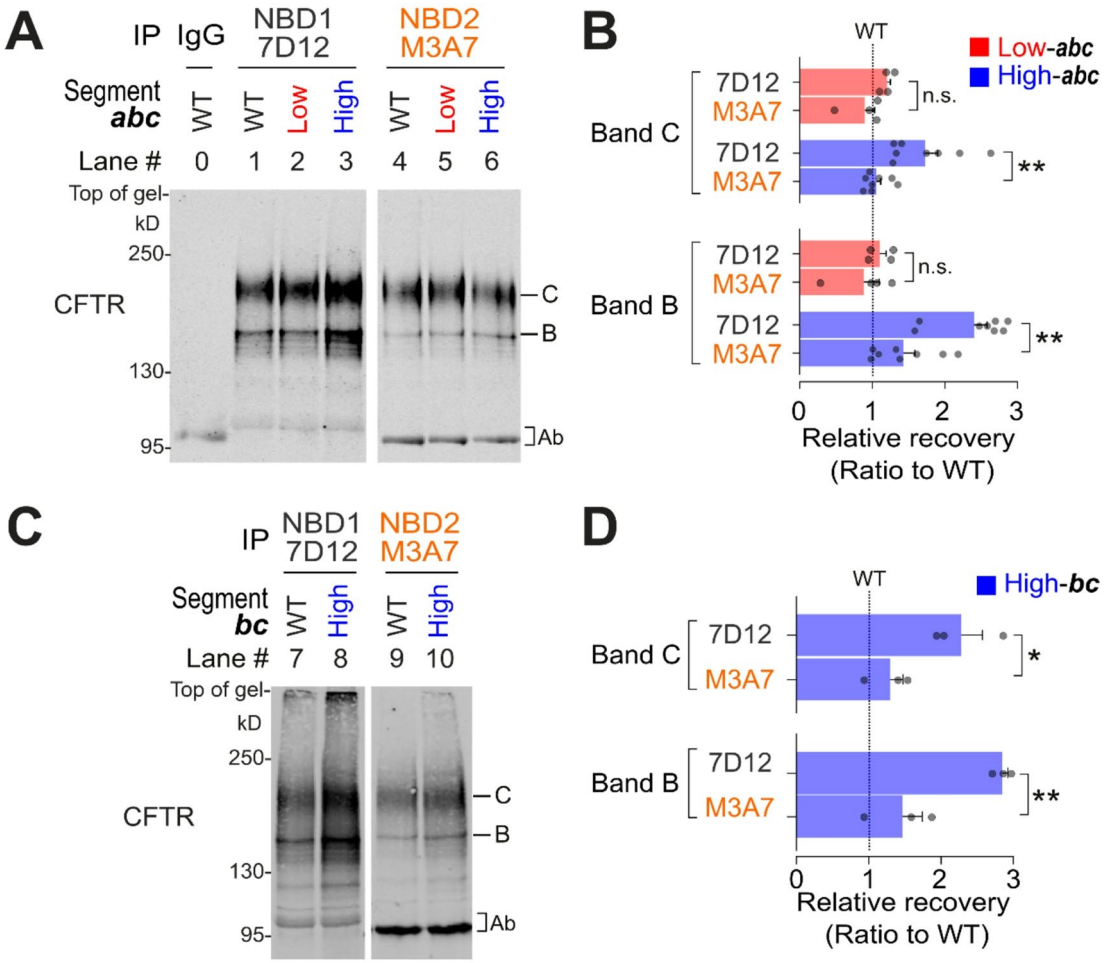

Fig. 5. Mature CFTR retains cotranslationally imprinted conformational properties in NBD1. (**A**) Representative immunoblot of WT and CFTR constructs with Low- and High-codons in segment-*abc* immunoprecipitated with anti-CFTR antibodies 7D12 and M3A7. Mouse immunoglobulin G (IgG) was used as a negative control. Immature (band B) and mature (band C) forms of CFTR protein are indicated. The original uncropped blot is presented in Fig. S6A. (**B**) Summary data show the fold changes in immature and mature CFTR protein of the CFTR constructs with Low- and High-codons in segment-*abc* relative to that of WT for the anti-CFTR antibodies 7D12 and M3A7. Symbols show individual values, and columns are means ± SEM ($n = 4$–8 independent experiments per variant); $^{**}P < 0.01$ vs. M3A7 (two-tailed Student's t-test). (**C**) Representative immunoblot of WT and the CFTR construct with High-codons in segment-*bc* immunoprecipitated with the anti-CFTR antibodies 7D12 and M3A7. For further information, see panel A. The original uncropped blot is presented in Fig. S6B. (**D**) Summary data show the fold changes in immature and mature CFTR protein of the CFTR construct with High-codons in segment-*bc* relative to WT for the anti-CFTR antibodies 7D12 and M3A7. Symbols show individual values, and columns are means ± SEM ($n = 3$ independent experiments); $^{*}P < 0.05$, $^{**}P < 0.01$ vs. M3A7 (two-tailed Student's t-test).

Discussion

This study reveals that biased codon usage within the CFTR CDS governs specific steps of NBD1 translation and folding, ultimately influencing the conformational and functional properties of full-length mature CFTR protein. We demonstrate that: (i) native codon bias induces a transient translation pause during a critical period of NBD1 synthesis (i.e. the formation of the parallel β-sheet core) which reduces the aggregation propensity of immature CFTR, (ii) disrupting this pause by selective synonymous codon substitutions increases off-pathway aggregation, (iii) these cotranslational events leave an imprint in conformational properties on the nascent protein that persists through maturation and trafficking to the plasma membrane, and (iv) the subtly altered CFTR exhibits enhanced functional properties characterized by increased affinity and efficacy of ATP-dependent channel gating. Collectively, our findings imply that biased codon usage has evolved to fine-tune NBD1 cotranslational folding to achieve a delicate balance between protein fitness (channel function) and off-pathway folding events (aggregation).

Native codon bias is generally considered to be adapted to protein needs rather than randomly distributed across the CDS, as exemplified by the enrichment of certain rare or inefficient codons near specific structural elements or boundaries[39,47]. The CFTR NBD1 domain, characterized by a complex folding process and high

contact order[12], appears to benefit from such codon-level regulation. Using a model based on predicted tRNA availability described by Spencer and Barral[21], we identified an enrichment of Low-efficiency codons within the α-helical subdomain of NBD1[19]. A comparative study by Pizzo et al.[48], employing the %MinMax algorithm, similarly identified conserved clusters of rare codons in this region across multiple species. These theoretical conjectures suggest that a translational sojourn specified by codon usage may affect NBD1 folding and, consequently, CFTR biogenesis. Our ribosome profiling data provide experimental validation of this concept, revealing that native codon bias transiently slows translation during the synthesis of the NBD1 α-helical subdomain (Figs. 1D and 2B).

Codon-resolution ribosome profiling further revealed multiple sites of transient ribosome stalling (translational pauses, arbitrarily defined) across the CFTR CDS (Figs. 2B and S3). These pauses appear to align with several key biosynthetic events, including the initial emergence of the nascent chain from the ribosome (residues 26 and 33), domain completion events (residues 375, 388, and 732), (core-)glycosylation (residue 948), and α-helical subdomain folding in both NBD1 (residue 558) and NBD2 (residue 1308). Unexpectedly, two specific codons, Leu(UUA) and Glu(GAA), were disproportionately associated with these sites of ribosomal pausing (Fig. 2B). However, as not all instances of these codons induced pauses (Fig. 2C), codon identity alone is unlikely to fully account for the observed variation in translation rate. Other regulatory factors, such as local nucleotide context, nascent peptide properties, mRNA secondary structure, RNA-binding proteins, and microRNAs, are likely to contribute to the modulation of codon-mediated translation rate[25,32,39,49].

By introducing synonymous codon substitutions designed to alter the translation rate within a limited segment of NBD1, we acquired compelling evidence to suggest that native codon usage reduces early off-pathway aggregation during CFTR biogenesis (Figs. 1B,C and 3B,C). Notably, a translational pause at Leu558 is a key determinant of CFTR aggregation propensity. Elimination of this pause, along with substitution of additional High-efficiency codons, markedly increased CFTR aggregation (Fig. 3). Given that the α-helical subdomain partially shields the hydrophobic core of NBD1 (Ile502, Cys524, Leu526, Leu541, and Ile556)[19], we propose that the translational pause at Leu558 temporally coordinates subdomain folding to minimize inappropriate exposure of these hydrophobic residues. Such exposure, when occurring in misfolded intermediates during CFTR biogenesis, may increase their susceptibility to aggregation or delay their clearance. Further studies are warranted to determine how the altered translation rate influences other cotranslational events, such as molecular chaperone recruitment and co-/post-translational modifications, and whether these perturbations contribute to changes in CFTR aggregation propensity, conformational maturation, or functional properties.

Despite the early off-target aggregation observed using the CFTR construct with High-codons in segment-*abc*, its overall processing and maturation efficiency were largely unaffected (Figs. 1B,C and 3B,C)[19]. The aggregation phenotype was subtle and only detectable in the RIPA-insoluble fraction of newly synthesized protein[19], suggesting that the effect was limited to early misfolded intermediates. Consistent with this idea, the High-codon construct exhibited ion conductance closely comparable to that of WT without the need for low-temperature incubation or CFTR correctors, suggesting that the codon substitutions had minimal impact on the domain assembly required for functional channel formation and allowed trafficking to the membrane. Nevertheless, altered 7D12 reactivity in this CFTR construct (Figs. 4 and 5) suggests that its folding trajectory deviates from that of WT in certain aspects, with such differences maintained through to the mature CFTR protein. It is important to note that the 7D12 antibody was raised against recombinant human NBD1 bearing the F508del mutation along with stabilizing suppressor mutations (G550E, R553M, and R555K) (cftrfolding.org), which may influence its conformational reactivity. Moreover, the 7D12 epitope (residues 531–540) resides in the Structurally Diverse Region (SDR; H4-H5 loop) of NBD1 (Figs. 1A, 4A, and 6A), a unique feature of CFTR among ATP-binding cassette (ABC) transporters[17]. Notably, Hoelen et al.[40] demonstrated that the SDRs of WT and F508del NBD1 exhibit different susceptibilities to proteolysis, supporting the notion that this region is particularly sensitive to folding changes. Given that NBD1 is a known hotspot for co- and post-translational covalent modifications[50,51], it is plausible that disruption of the native translational pause near Leu558 transiently alters the accessibility of the nascent chain or its susceptibility to modifications. Such changes may affect the conformational properties of the SDR and antibody accessibility, offering a possible explanation for the persistent differences observed in the High-codon construct. However, several limitations should be considered when interpreting the IP experiments: (i) the use of epitope-specific antibodies (3G11, 7D12, and UNC660) may have missed conformational changes outside the targeted regions, and (ii) the observed changes may reflect a subpopulation of newly synthesized protein rather than the entire pool. Although direct structural analysis could, in principle, provide additional insight, such approaches face significant technical limitations. In particular, if the conformational change arises from post-translational modifications occurring only in a subset of newly synthesized proteins, it would be extremely challenging to detect using ensemble structural methods, which average signals across heterogeneous populations and may fail to resolve subtle differences. Therefore, while structural data could be informative, it is unlikely to definitively capture the specific changes observed in this context.

To address these limitations and assess the functional relevance of codon usage-induced conformational changes, we performed single-channel recording, which provides an independent assessment of CFTR behavior while providing complementary evidence for persistent effects of codon usage changes in the CFTR construct with High-codons in segment-*abc*. Single-channel recordings from two independent laboratories demonstrated that the CFTR construct with High-codons in segment-*abc* exhibits enhanced channel gating compared to WT (Fig. 6D and G). Because the SDR (7D12 epitope region) may influence interdomain contacts between NBD1 and NBD2, and hence, NBD dimerization[52], it is plausible that conformational changes in this segment might contribute to the increased P_o of the channel. This could occur by enhanced affinity of ATP binding, increased stability of the NBD1-NBD2 dimer, and/or a reduced rate of ATP hydrolysis, each of which could in turn contribute to the observed augmented frequency and duration of channel openings[42,53]. Additionally, although ribosome profiling did not reveal notable changes in the R domain of the CFTR constructs with High-

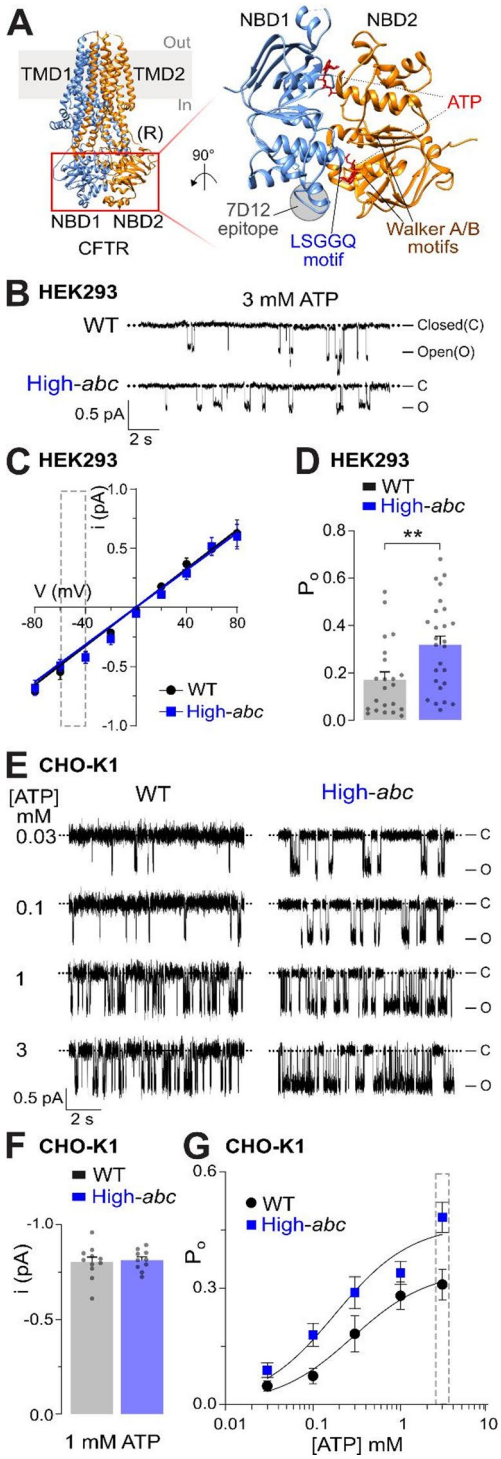

codons (Fig. S3), it remains possible that allosteric effects, such as altered phosphorylation of the R domain, could influence channel gating[52,54]. Regardless of the underlying mechanism, it is intriguing to note that channel activity can be improved by manipulating native codon usage, which may have evolved to favor a cotranslational folding pathway that prioritizes folding fidelity over maximal function. From a broader perspective, this observation suggests that CFTR codon usage has adapted to balance protein folding fidelity, particularly avoiding aggregation, with a trade-off in maximal channel activity.

The natural codon evolution demonstrated here has implications for the use of algorithms frequently employed to optimize CFTR sequences in genetic mRNA and/or DNA replacement therapies. First, optimizing the CFTR sequence to achieve desired parameters, such as increased protein synthesis or improved function, may result in unforeseen consequences that could have potentially harmful effects. Second, certain codon regions are much more likely to exert effects than others, even when they are closely positioned. Third, it remains challenging to accurately predict where such codons exist, how they elicit their desired effects, and what spectrum of consequences might result from specific changes.

◀**Fig. 6**. Cotranslational imprinting in NBD1 influences CFTR channel gating. (**A**) Location of the 7D12 antibody epitope relative to the ATP-binding sites at the NBD1-NBD2 dimer interface. Left, orthogonal representation of phosphorylated, ATP-bound human CFTR with the E1371Q mutation (Fig. 1A) and the NBD1-NBD2 dimer indicated by a red box. Right, magnified view of the NBD1-NBD2 dimer rotated 90° about the y-axis to highlight the position of the 7D12 epitope (grey circle) relative to the Walker A and B motifs in NBD2 and the LSGGQ (ABC signature) motif in NBD1, which together form ATP-binding site 2 (hydrolytic). NBD1 and NBD2 are colored light blue and orange, respectively, while the ATP molecules are colored red. (**B**–**D**) [Blind study 1, Yonsei University] Measurement of CFTR Cl^- channel activity in HEK293 cells. (**B**) Representative single-channel recordings of WT CFTR and the CFTR construct with High-codons in segment-*abc* made with excised inside-out membrane patches bathed in symmetrical 150 mM Cl^- solutions voltage-clamped at –60 mV. MgATP (3 mM) and recombinant PKA (10 U/ml) were continuously present in the intracellular solution and temperature was 20–23 °C. The open (O) and closed (**C**) channel states are indicated. (**C**) Single-channel current–voltage (i–V) relationships of WT CFTR and the CFTR construct with High-codons in segment-*abc* using the recording conditions described in panel B. Data are means ± SEM (n = 8–11 independent experiments). Error bars are smaller than symbol size except where shown. The continuous lines are the fit of first-order functions to mean data. A dashed box highlights the − 60 to − 40 mV range to facilitate comparison with the corresponding data in panel F. (**D**) Open probability (P_o) of WT CFTR and the CFTR construct with High-codons in segment-*abc* using the recording conditions described in panel B. Symbols show individual values and columns are means ± SEM ($n = 22–26$ replicates); $^{**}P < 0.01$ vs. WT CFTR (two-tailed Student's t-test). (**E**–**G**) [Blind study 2, University of Bristol] Measurement of CFTR Cl^- channel activity in CHO-K1 cells. (**E**) Representative recordings show the single-channel activity of WT CFTR and the CFTR construct with High-codons in segment-*abc* in excised inside-out membrane patches. The recordings were made in the continuous presence of purified PKA (75 nM) and the indicated concentrations of ATP in the intracellular solution. Excised inside-out membrane patches were voltage-clamped at − 50 mV in the presence of a large Cl^- concentration gradient ($[Cl^-]_{internal} = 147$ mM, $[Cl^-]_{external} = 10$ mM) and temperature was 37 °C. The open (O) and closed (C) channel states are indicated. (**F**) Single-channel current amplitude of WT CFTR and the CFTR construct with High-codons in segment-*abc* measured using the recording conditions described in panel E with ATP (1 mM) in the intracellular solution. Symbols show individual values and columns are means ± SEM ($n = 11–10$ replicates). (**G**) Relationship between ATP concentration and P_o for WT CFTR and the CFTR construct with High-codons in segment-*abc* using the recording conditions described in panel E. Data are means ± SEM ($n \geq 6$ replicates per ATP concentration). The continuous lines are the fit of Michaelis–Menten functions to mean data. A dashed box highlights the data points at 3 mM ATP to facilitate comparison with the corresponding data in panel D.

An important caveat of this study is that CFTR was exogenously overexpressed in non-epithelial cells. We selected this system for several practical reasons: (i) it allowed efficient expression of cDNA-based constructs bearing multiple synonymous codon substitutions (ten constructs in this study); (ii) HEK293 and CHO-K1 cells, which lack endogenous CFTR expression, are widely used for exogenous protein expression; (iii) overexpression yielded sufficient CFTR expression for both single-transcript ribosome profiling and single-channel studies; and (iv) the use of cDNA minimized complications arising from alternative splicing of the CFTR transcript[55,56], which can pose challenges in ribosome profiling analyses. However, we acknowledge that this experimental system does not fully recapitulate the molecular environment of CFTR-expressing epithelial cells. Cell type-specific factors, including tRNA availability, mRNA secondary structure and modifications, chaperone abundance, and co/post-translational modifications, may influence CFTR translation, folding, maturation, and function in its native cellular context. Furthermore, our study did not assess whether synonymous codon substitutions affect CFTR localization at the plasma membrane or its activity in intact cells. Instead, we focused on intrinsic channel function using single-channel recording. This approach was chosen to minimize confounding effects from additional cellular factors, such as ion gradients and regulatory proteins, that can influence CFTR activity in intact cells[14,57].

Taken together, our findings support the conclusion that native codon usage in CFTR modulates translation rate at specific points during protein synthesis, thereby affecting the cotranslational folding pathway of CFTR. This process imprints specific conformational properties onto the nascent polypeptide, ultimately influencing key aspects of protein fitness, including folding efficiency, aggregation propensity, and channel function. While the principles identified here provide an important consideration when attempting to "optimize" the CFTR CDS for genetic therapies, further studies are needed to more precisely determine how synonymous changes influence protein biogenesis and function in native epithelial cells.

Methods

Plasmid constructs, cell culture, and transient expression

Synonymous codon substitutions were introduced into the mammalian expression plasmids pcDNA3-CFTR and pcDNA3-CFTR NBD1[4] by PCR overlap extension with synthetic oligonucleotides as previously described[19]. All modified regions were verified by Sanger sequencing.

Human embryonic kidney (HEK) 293 cells (RRID:CVCL_0045) and Chinese hamster ovary K1 (CHO-K1) cells (RRID:CVCL_0214) were obtained from the American Type Culture Collection (ATCC; HEK293: Cat# CRL-1573, CHO-K1: Cat# CCL-61) and maintained at 37 °C in a humidified atmosphere of 5% CO_2. HEK293 cells were cultured in Dulbecco's modified Eagle's medium (DMEM) supplemented with 10% fetal calf serum,

100 U ml^{-1} penicillin, and 100 µg ml^{-1} streptomycin (Life Technologies), and CHO-K1 cells were cultured in Ham's F-12 medium with the same supplements.

Cells were transiently transfected with plasmid DNA using Lipofectamine (Life Technologies). For immunoblotting, immunoprecipitation, and metabolic labeling experiments, HEK293 cells were harvested 24 h (NBD) or 48 h (CFTR) post-transfection. Transfection efficiency was confirmed by co-transfection with pEGFP-N3 (Clontech) and GFP immunoblotting. For single-channel studies, HEK293 or CHO-K1 cells were co-transfected with CFTR constructs and GFP and 36–60 h later GFP-positive cells were selected for study using the patch-clamp technique.

Immunoblotting and immunoprecipitation

Cells were lysed in 600 µl of ice-cold RIPA buffer [50 mM Tris–HCl/pH 8.0, 150 mM NaCl, 1 mM EDTA, 1% (v/v) Triton X-100, 0.5% (w/v) sodium deoxycholate, 0.1% (w/v) SDS] supplemented with cOmplete protease inhibitors (Roche). Lysates were incubated on ice for 15 min and centrifuged at 16,000 × *g* for 15 min at 4 °C. The RIPA-insoluble pellet was rinsed with Dulbecco's phosphate-buffered saline (PBS; Invitrogen), resuspended in 20 µl of 20 mM Tris–HCl/pH 7.4 containing 1% (w/v) SDS, incubated at room temperature for 20 min, and then diluted with 180 µl RIPA buffer.

For immunoprecipitation, RIPA-soluble lysates were incubated overnight at 4 °C with one of the following antibodies: rat anti-CFTR 3G11 (CFTR Folding Consortium), mouse anti-CFTR 7D12 (CFTR Folding Consortium), mouse anti-CFTR UNC660 (CFTR Antibody Distribution Program of the Cystic Fibrosis Foundation), or mouse anti-CFTR antibody M3A7 (Millipore, Cat# MAB3480, RRID:AB_2081244). Immune complexes were captured with Affi-Gel Protein G beads (Bio-Rad) for 2 h at 4 °C, washed three times with RIPA buffer and twice with Tris-buffered saline [20 mM Tris–HCl/pH 7.5, 137 mM NaCl], and then prepared for SDS–polyacrylamide gel electrophoresis (PAGE).

Proteins were separated by SDS-PAGE and transferred to polyvinylidene fluoride (PVDF) membranes (Millipore). Membranes were probed with primary antibodies (rat anti-CFTR 3G11, mouse anti-CFTR M3A7, rabbit anti-β-actin (Cell Signaling Technology, Cat# 4967, RRID:AB_330288), or rabbit anti-GFP (Clontech, Cat# 632592, RRID:AB_10013427), followed by appropriate secondary antibodies. Immunoblots were visualized using the Odyssey Infrared Imaging System (LI-COR) or ChemiDoc XRS+ System (Bio-Rad) and analyzed with the accompanying image analysis software.

Metabolic radiolabeling

HEK293 cells were transiently transfected and incubated for 24 h. Cells were rinsed once with 37 °C PBS, incubated in methionine- and cysteine-free medium for 30 min, and then labeled with 30 µCi Trans^{35}S-label (MP Biomedicals) per well for 15 min. Radiolabeling was terminated by rinsing cells with ice-cold PBS, followed by snap-freezing in liquid nitrogen. Frozen cells were thawed at room temperature and lysed in RIPA buffer for 15 min at 4 °C. Cell debris was removed by centrifugation at 16,000 × *g* for 15 min at 4 °C, and cleared lysates were subjected to IP. After separation on SDS-PAGE, the radiolabeled bands were visualized and analyzed using the Personal FX phosphor imager and Quantity One software (Bio-Rad).

Ribosome footprint profiling—library preparation

HEK293 cells transiently transfected with CFTR constructs were cultured in DMEM supplemented with 10% fetal calf serum for 24 h without penicillin–streptomycin. Ribosome profiling libraries were prepared as described[58,59] with a few modifications. In brief, cells were rapidly chilled by rinsing with ice-cold PBS, lysed in ice-cold lysis buffer [20 mM Tris–HCl/pH 7.4, 150 mM NaCl, 5 mM $MgCl_2$, 1 mM dithiothreitol (DTT), 1% (v/v) Triton X-100, and 25 U ml^{-1} Turbo DNase I] for 10 min on ice, and then triturated ten times through a 26-G needle. After clearance by centrifugation at 16,000 g for 10 min at 4 °C, the lysates were digested with 100 U RNase I (Ambion) per A_{260} lysate for 45 min at room temperature with gentle agitation prior to adding 200 U RiboLock RNase Inhibitor (Thermo Fisher Scientific).

Ribosome protected mRNA fragments were isolated by ultracentrifugation through a 1 M sucrose cushion in polysome buffer [20 mM Tris–HCl/pH 7.4, 150 mM NaCl, 7.5 mM $MgCl_2$, 0.5 mM DTT, 20 U ml^{-1} RiboLock RNase Inhibitor] at 70,000 rpm for 2 h at 4 °C using a TLA-110 rotor (Beckman Coulter). Ribosome pellets were extracted using TRIzol (Invitrogen), and RNA fragments were separated by electrophoresis on a 12% (w/v) denaturing polyacrylamide gel with 8 M urea. RNA fragments with sizes ranging from 26 to 34 nt were manually excised from the SYBR Gold (Invitrogen)-stained gels and purified.

3′-Oligonucleotide adaptor ligation, reverse transcription, circularization, and rRNA depletion using biotinylated oligonucleotides were performed as described previously[58,59]. Libraries were barcoded using indexing primers for each sample during PCR amplification. Barcoded libraries were then pooled with 3% (v/v) PhiX (Illumina) and sequenced on a NextSeq 500 platform (Illumina) as per the manufacturer's protocol to yield ~ 30–60 million reads per sample.

Ribosome footprint profiling—data analysis

Sequencing reads were first trimmed to remove 3′ adaptors and mapped to human rRNA sequences (RNA5S1, RefSeq: NR_023363; RNA5-8SN5, RefSeq: NR_003285; RNA18SN5, RefSeq: NR_003286 and RNA28SN5, RefSeq: NR_003287) using HISAT (RRID:SCR_015530)[60] to eliminate rRNA contaminant reads. The remaining reads were aligned to the CFTR construct sequence and the longest transcript variant of each human gene in GRCh38, excluding CFTR. A maximum of two mismatches at the 5′ end of reads was allowed. The 5′ end nucleotide from each read was annotated and mapped onto each transcript, and all multi-mapped reads were discarded.

Ribosome footprints with lengths between 28 to 30 nt were utilized for triplet periodicity analysis and CFTR ribosome profiling. For CFTR ribosome profiling, only footprints mapped onto the first base of a codon (Frame-0) in the CDS of CFTR constructs were used. Three nucleotide sequences positioned 16th-18th from the 5′ end of each footprint were defined as a codon occupying the ribosomal A-site (A-site codon)[35,61] and the A-site position of each footprint was used to infer the position of the ribosome on the CFTR transcript. Processing of sequencing data was performed on the Galaxy platform (RRID:SCR_006281)[62].

Electrophysiology

[Blind study 1, Yonsei University] Glass coverslips with transfected HEK293 cells were transferred to a chamber on the stage of an inverted microscope (IX71, Olympus). Patch pipettes were fabricated from borosilicate glass capillaries (TW150F-4 from World Precision Instruments) and fire polished to achieve electrode resistances of 15 – 20 MΩ for single-channel recording. The bath (intracellular) solution contained (in mM): 148 *N*-methyl-D-glucamine (NMDG)-Cl, 1 $MgCl_2$, 5 EGTA, and 10 HEPES (pH 7.4). The pipette (extracellular) solution contained (in mM): 146 NMDG-Cl, 1 $MgCl_2$, 1 $CaCl_2$, 10 D-(+)-Glucose, and 10 HEPES (pH 7.4). For single-channel studies of CFTR using inside-out membrane patches, membrane potential was clamped at −60 mV except when acquiring data for current–voltage (i–V) relationships when membrane potential was stepped from −80 to +80 mV in 20 mV increments. CFTR channels were activated by adding 3 mM MgATP and 10 U/ml PKA catalytic subunit (Promega) to the bath solution after patch excision. All experiments were performed at room temperature (20–23 °C). Command potential and data acquisition were controlled by pClamp 10.6 software (RRID:SCR_011323) (Molecular Devices). CFTR currents were recorded using an Axopatch 200B patch-clamp amplifier (Molecular Devices), filtered with a lowpass Bessel filter at 1 kHz and digitized by a Digidata 1550B (Molecular Devices). The gap-free data acquisition protocol was conducted with the pClamp software, Axoscope, at a sampling rate of 10 kHz. CFTR recordings were further filtered at a 100 Hz cutoff frequency for data analysis and presentation. For data analysis, single-channel current amplitude (i) was measured either manually using cursors to distinguish the open and closed channel levels or by constructing all-points histograms and fitting these with Gaussian functions. P_o was determined by generating events lists using a half-amplitude crossing criterion and analyzing them using Clampfit 10.6 software (Molecular Devices).

[Blind study 2, University of Bristol] CFTR Cl^- channels were recorded in excised inside-out membrane patches using an Axopatch 200B patch-clamp amplifier and pCLAMP software (version 10) (both from Molecular Devices)[63]. The pipette (extracellular) solution contained (mM): 140 NMDG, 140 aspartic acid, 5 $CaCl_2$, 2 $MgSO_4$ and 10 *N*-tris[hydroxymethyl]methyl-2-aminoethanesulfonic acid (TES), adjusted to pH 7.3 with Tris ($[Cl^-]$, 10 mM). The bath (intracellular) solution contained (mM): 140 NMDG, 3 $MgCl_2$, 1 CsEGTA and 10 TES, adjusted to pH 7.3 with HCl ($[Cl^-]$, 147 mM; free $[Ca^{2+}]$, $< 10^{-8}$ M) and was maintained at 37 °C. After excision of inside-out membrane patches, the catalytic subunit of protein kinase A (PKA; 75 nM) and ATP (1 mM) were added to the intracellular solution within 2 min of patch excision to activate CFTR Cl^- channels. To minimize channel rundown, PKA and ATP were added to all intracellular solutions and voltage was clamped at −50 mV. To investigate ATP concentration–response relationships, data were acquired from membrane patches where at least 3 ATP concentrations were tested and the reference concentration (1 mM ATP) studied at least twice. In this study, membrane patches contained ≤ 5 active channels. To determine channel number, the maximum number of simultaneous channel openings observed during an experiment was determined[64]. To minimize errors, experimental conditions were used that robustly stimulate channel activity and recordings were verified to be of sufficient length to ascertain the correct number of channels. Single channel records were filtered with an eight-pole Bessel filter (model F-900C/9L8L, Frequency Devices Inc.) at a corner frequency (f_c) of 500 Hz and digitized using a DigiData 1320A interface (Molecular Devices) and pCLAMP software at a sampling rate of 5 kHz. To measure i, Gaussian distributions were fit to current amplitude histograms. To determine P_o, lists of open- and closed-times were created using a half-amplitude crossing criterion for event detection and dwell-time histograms constructed and fitted with one or more component exponential functions using the maximum likelihood method; transitions < 1 ms were excluded from the analysis (eight-pole Bessel filter rise time ($T_{10\text{-}90}$) ~ 0.73 ms at f_c = 500 Hz). For the purpose of illustration, single-channel records were filtered at 500 Hz and digitized at 5 kHz before file size compression by fivefold data reduction.

PKA purified from bovine heart was purchased from Calbiochem (now Merck Life Science UK Ltd.). All other chemicals were of reagent grade and supplied by Sigma-Aldrich Ltd. (now Merck Life Science UK Ltd.). Stock solutions of ATP, dissolved in intracellular solution, were prepared fresh before each experiment. Immediately before use, stock solutions of ATP were diluted to final concentrations and, where necessary, the pH of the intracellular solution was readjusted to pH 7.3 to avoid pH-dependent changes in CFTR function[44].

Statistics

Data recording and analyses were randomized with electrophysiological studies additionally blinded. Results are expressed as means ± SEM of n observations, but some group sizes were unequal due to technical difficulties with the acquisition of single-channel data. To test for differences between two groups of data, Student's unpaired t-test was used. Tests were performed with either Prism 9 (RRID:SCR_002798; GraphPad Software) or SigmaPlot (version 13.0; RRID:SCR_003210; Systat Software Inc.). Differences were considered statistically significant when $P < 0.05$. To avoid pseudo-replication, all experiments were repeated at different times.

Data availability

The ribosome profiling datasets generated and/or analysed during the current study are available in the Gene Expression Omnibus (GEO) database, [GSE305005].

Received: 20 August 2025; Accepted: 1 December 2025

Published online: 12 December 2025

References

1. Anfinsen, C. B. Principles that govern the folding of protein chains. *Science* **181**, 223–230 (1973).
2. Wruck, F., Katranidis, A., Nierhaus, K. H., Büldt, G. & Hegner, M. Translation and folding of single proteins in real time. *Proc. Natl. Acad. Sci. U. S. A.* **114**, E4399–E4407 (2017).
3. Liutkute, M., Maiti, M., Samatova, E., Enderlein, J. & Rodnina, M. V. Gradual compaction of the nascent peptide during cotranslational folding on the ribosome. *Elife* **9**, 1–21 (2020).
4. Matsumura, Y., David, L. L. & Skach, W. R. Role of Hsc70 binding cycle in CFTR folding and endoplasmic reticulum–associated degradation. *Mol. Biol. Cell* **22**, 2797–2809 (2011).
5. Komar, A. A., Samatova, E. & Rodnina, M. V. Translation rates and protein folding. *J. Mol. Biol.* **436**, 168384 (2024).
6. Chen, X., Hilser, V. J. & Kaiser, C. M. Arrest peptide profiling resolves co-translational folding pathways and chaperone interactions in vivo. *Nat. Commun.* **16**, 6833 (2025).
7. Cabrita, L. D. et al. A structural ensemble of a ribosome-nascent chain complex during cotranslational protein folding. *Nat. Struct. Mol. Biol.* **23**, 278–285 (2016).
8. Bitran, A., Jacobs, W. M., Zhai, X. & Shakhnovich, E. Cotranslational folding allows misfolding-prone proteins to circumvent deep kinetic traps. *Proc. Natl. Acad. Sci. U. S. A.* **117**, 1485–1495 (2020).
9. Kleizen, B., van Vlijmen, T., de Jonge, H. R. & Braakman, I. Folding of CFTR is predominantly cotranslational. *Mol. Cell.* **20**, 277–287 (2005).
10. Zhang, Z., Liu, F. & Chen, J. Molecular structure of the ATP-bound, phosphorylated human CFTR. *Proc. Natl. Acad. Sci. U. S. A.* **115**, 12757–12762 (2018).
11. Im, J. et al. ABC-transporter CFTR folds with high fidelity through a modular, stepwise pathway. *Cell. Mol. Life Sci.* **80**, 33 (2023).
12. Kim, S. J. & Skach, W. R. Mechanisms of CFTR folding at the endoplasmic reticulum. *Front. Pharmacol.* **3**, 201 (2012).
13. Rabeh, W. M. et al. Correction of both NBD1 energetics and domain interface is required to restore ΔF508 CFTR folding and function. *Cell* **148**, 150–163 (2012).
14. Farinha, C. M., Santos, L. & Ferreira, J. F. Cell type-specific regulation of CFTR trafficking-on the verge of progress. *Front. Cell. Dev. Biol.* **12**, 1338892 (2024).
15. Thibodeau, P. H. et al. The cystic fibrosis-causing mutation ΔF508 affects multiple steps in cystic fibrosis transmembrane conductance regulator biogenesis. *J. Biol. Chem.* **285**, 35825–35835 (2010).
16. Mendoza, J. L. et al. Requirements for efficient correction of ΔF508 CFTR revealed by analyses of evolved sequences. *Cell* **148**, 164–174 (2012).
17. Lewis, H. A. et al. Structure of nucleotide-binding domain 1 of the cystic fibrosis transmembrane conductance regulator. *EMBO J.* **23**, 282–293 (2004).
18. Khushoo, A., Yang, Z., Johnson, A. E. & Skach, W. R. Ligand-driven vectorial folding of ribosome-bound human CFTR NBD1. *Mol. Cell.* **41**, 682–692 (2011).
19. Kim, S. J. et al. Translational tuning optimizes nascent protein folding in cells. *Science* **348**, 444–448 (2015).
20. Shishido, H., Yoon, J. S., Yang, Z. & Skach, W. R. CFTR trafficking mutations disrupt cotranslational protein folding by targeting biosynthetic intermediates. *Nat. Commun.* **11**, 4258 (2020).
21. Spencer, P. S. & Barral, J. M. Genetic code redundancy and its influence on the encoded polypeptides. *Comput. Struct. Biotechnol. J.* **1**, e201204006 (2012).
22. Yu, C.-H. et al. Codon usage influences the local rate of translation elongation to regulate co-translational protein folding. *Mol. Cell.* **59**, 744–754 (2015).
23. Oliver, K. E. et al. Slowing ribosome velocity restores folding and function of mutant CFTR. *J. Clin. Invest.* **129**, 5236–5253 (2019).
24. Tao, P. & Xiao, Y. Pathway regulation mechanism by cotranslational protein folding. *Commun. Chem.* **8**, 226 (2025).
25. Collart, M. A. & Weiss, B. Ribosome pausing, a dangerous necessity for co-translational events. *Nucleic Acids Res.* **48**, 1043–1055 (2020).
26. Drummond, D. A. & Wilke, C. O. Mistranslation-induced protein misfolding as a dominant constraint on coding-sequence evolution. *Cell* **134**, 341–352 (2008).
27. Simms, C. L., Yan, L. L., Qiu, J. K. & Zaher, H. S. Ribosome collisions result in +1 frameshifting in the absence of no-go decay. *Cell. Rep.* **28**, 1679-1689.e4 (2019).
28. Mishima, Y., Han, P., Ishibashi, K., Kimura, S. & Iwasaki, S. Ribosome slowdown triggers codon-mediated mRNA decay independently of ribosome quality control. *EMBO J.* **41**, e109256 (2022).
29. Hou, W., Harjono, V., Harvey, A. T., Subramaniam, A. R. & Zid, B. M. Quantification of elongation stalls and impact on gene expression in yeast. *RNA* **29**, 1928–1938 (2023).
30. Sander, I. M., Chaney, J. L. & Clark, P. L. Expanding Anfinsen's principle: Contributions of synonymous codon selection to rational protein design. *J. Am. Chem. Soc.* **136**, 858–861 (2014).
31. Hanson, G. & Coller, J. Codon optimality, bias and usage in translation and mRNA decay. *Nat. Rev. Mol. Cell. Biol.* **19**, 20–30 (2018).
32. Liu, Y. A code within the genetic code: Codon usage regulates co-translational protein folding. *Cell. Commun. Signal* **18**, 145 (2020).
33. Plessa, E. et al. Nascent chains can form co-translational folding intermediates that promote post-translational folding outcomes in a disease-causing protein. *Nat. Commun.* **12**, 6447 (2021).
34. Davyt, M., Bharti, N. & Ignatova, Z. Effect of mRNA/tRNA mutations on translation speed: Implications for human diseases. *J. Biol. Chem.* **299**, 105089 (2023).
35. Ingolia, N. T., Ghaemmaghami, S., Newman, J. R. S. S. & Weissman, J. S. Genome-wide analysis in vivo of translation with nucleotide resolution using ribosome profiling. *Science* **324**, 218–223 (2009).
36. Ingolia, N. T., Brar, G. A., Rouskin, S., McGeachy, A. M. & Weissman, J. S. The ribosome profiling strategy for monitoring translation in vivo by deep sequencing of ribosome-protected mRNA fragments. *Nat. Protoc.* **7**, 1534–1550 (2012).
37. Gerashchenko, M. V. & Gladyshev, V. N. Translation inhibitors cause abnormalities in ribosome profiling experiments. *Nucleic Acids Res.* **42**, e134 (2014).
38. Ingolia, N. T., Hussmann, J. A. & Weissman, J. S. Ribosome profiling: Global views of translation. *Cold Spring Harb. Perspect. Biol.* **11**, a032698 (2019).
39. Liu, Y., Yang, Q. & Zhao, F. Synonymous but not silent: The codon usage code for gene expression and protein folding. *Annu. Rev. Biochem.* **90**, 375–401 (2021).
40. Hoelen, H. et al. The primary folding defect and rescue of ΔF508 CFTR emerge during translation of the mutant domain. *PLoS ONE* **5**, e15458 (2010).
41. Peters, K. W. et al. CFTR Folding Consortium: Methods available for studies of CFTR folding and correction. *Methods Mol. Biol.* **742**, 335–353 (2011).
42. Vergani, P., Lockless, S. W., Nairn, A. C. & Gadsby, D. C. CFTR channel opening by ATP-driven tight dimerization of its nucleotide-binding domains. *Nature* **433**, 876–880 (2005).

43. Jih, K.-Y., Sohma, Y. & Hwang, T.-C. Nonintegral stoichiometry in CFTR gating revealed by a pore-lining mutation. *J. Gen. Physiol.* **140**, 347–359 (2012).
44. Chen, J. H., Cai, Z. & Sheppard, D. N. Direct sensing of intracellular pH by the cystic fibrosis transmembrane conductance regulator (CFTR) Cl^- channel. *J. Biol. Chem.* **284**, 35495–35506 (2009).
45. Wang, Y., Cai, Z., Gosling, M. & Sheppard, D. N. Potentiation of the cystic fibrosis transmembrane conductance regulator Cl^- channel by ivacaftor is temperature independent. *Am. J. Physiol. Lung Cell. Mol. Physiol.* **315**, L846–L857 (2018).
46. Mihályi, C., Iordanov, I., Szollosi, A. & Csanády, L. Structural determinants of protein kinase A essential for CFTR channel activation. *Proc. Natl. Acad. Sci. U. S. A.* **121**, e2407728121 (2024).
47. Chaney, J. L. et al. Widespread position-specific conservation of synonymous rare codons within coding sequences. *PLoS Comput. Biol.* **13**, e1005531 (2017).
48. Pizzo, L., Iriarte, A., Alvarez-Valin, F. & Marín, M. Conservation of CFTR codon frequency through primates suggests synonymous mutations could have a functional effect. *Mutat. Res.* **775**, 19–25 (2015).
49. Schuller, A. P. & Green, R. Roadblocks and resolutions in eukaryotic translation. *Nat. Rev. Mol. Cell. Biol.* **19**, 526–541 (2018).
50. McClure, M. L., Wen, H., Fortenberry, J., Hong, J. S. & Sorscher, E. J. S-palmitoylation regulates biogenesis of core glycosylated wild-type and F508del CFTR in a post-ER compartment. *Biochem. J.* **459**, 417–425 (2014).
51. Pankow, S., Bamberger, C. & Yates, J. R. A posttranslational modification code for CFTR maturation is altered in cystic fibrosis. *Sci. Signal* **12**, eaan7984 (2019).
52. Chong, P. A., Kota, P., Dokholyan, N. V. & Forman-Kay, J. D. Dynamics intrinsic to cystic fibrosis transmembrane conductance regulator function and stability. *Cold Spring Harb. Perspect. Med.* **3**, a009522 (2013).
53. Li, C. et al. ATPase activity of the cystic fibrosis transmembrane conductance regulator. *J. Biol. Chem.* **271**, 28463–28468 (1996).
54. Bozoky, Z. et al. Regulatory R region of the CFTR chloride channel is a dynamic integrator of phospho-dependent intra- and intermolecular interactions. *Proc. Natl. Acad. Sci. U. S. A.* **110**, E4427–E4436 (2013).
55. Buratti, E. et al. Nuclear factor TDP-43 and SR proteins promote in vitro and in vivo CFTR exon 9 skipping. *EMBO J.* **20**, 1774–1784 (2001).
56. Aissat, A. et al. Combined computational-experimental analyses of CFTR exon strength uncover predictability of exon-skipping level. *Hum. Mutat.* **34**, 873–881 (2013).
57. Saint-Criq, V. & Gray, M. A. Role of CFTR in epithelial physiology. *Cell. Mol. Life Sci.* **74**, 93–115 (2017).
58. Lueck, J. D. et al. Engineered transfer RNAs for suppression of premature termination codons. *Nat. Commun.* **10**, 822 (2019).
59. Wu, I.-H. et al. A role for the ribosome-associated complex in activation of the IRE1 branch of UPR. *Cell. Rep.* **35**, 109217 (2021).
60. Kim, D., Langmead, B. & Salzberg, S. L. HISAT: A fast spliced aligner with low memory requirements. *Nat. Methods* **12**, 357–360 (2015).
61. Guydosh, N. R. & Green, R. Dom34 rescues ribosomes in 3' untranslated regions. *Cell* **156**, 950–962 (2014).
62. Galaxy Community. The Galaxy platform for accessible, reproducible and collaborative biomedical analyses: 2022 update. *Nucleic Acids Res.* **50**, W345–W351 (2022).
63. Cai, Z. et al. Impact of the F508del mutation on ovine CFTR, a Cl^- channel with enhanced conductance and ATP-dependent gating. *J. Physiol.* **593**, 2427–2446 (2015).
64. Cai, Z., Taddei, A. & Sheppard, D. N. Differential sensitivity of the cystic fibrosis (CF)-associated mutants G551D and G1349D to potentiators of the cystic fibrosis transmembrane conductance regulator (CFTR) Cl^- channel. *J. Biol. Chem.* **281**, 1970–1977 (2006).
65. Pettersen, E. F. et al. UCSF Chimera—A visualization system for exploratory research and analysis. *J. Comput. Chem.* **25**, 1605–1612 (2004).

Acknowledgements

We thank Z. Yang for generating CFTR constructs and L. Rooney for initial guidance and suggestions on ribosome profiling. We are grateful to the CFTR Folding Consortium and the CFTR Antibody Distribution Program of the Cystic Fibrosis Foundation, as well as the laboratories of Dr. J. Riordan and Dr. M. Gentzsch (University of North Carolina at Chapel Hill), for providing CFTR antibodies. We acknowledge the Resource for Biocomputing, Visualization, and Informatics at the University of California, San Francisco, for the UCSF Chimera package. We also thank former and current members of our laboratories for insightful discussions and assistance, especially M. Mense and M. Rodrat.

Author contributions

Research design: JSY, HL, YK, HS, DNS, MGL, and WRS; Performed the research: JSY, HL, and YK; Data analysis and interpretation: JSY, HL, YK, HS, DNS, MGL, and WRS; Manuscript writing: JSY, DNS, and WRS; All authors have read and approved the final version of this manuscript.

Funding

This work was supported by the Cystic Fibrosis Foundation (SKACH05X0 to W.R.S. and SHEPPA14XX0 to D.N.S.), the National Institutes of Health (DK51818 and GM53457 to W.R.S.), and the National Research Foundation of Korea funded by the Ministry of Science and ICT (RS-2022-NR070524 to M.G.L).

Declarations

Competing interests

The authors declare no competing interests.

Additional information

Supplementary Information The online version contains supplementary material available at https://doi.org/10.1038/s41598-025-31274-w.

Correspondence and requests for materials should be addressed to J.S.Y., D.N.S. or W.R.S.